Role of the N-terminus in permeability of chicken connexin45.6 gap junctional channels

Lixian Dong[1], Xiaoqin Liu[1], Hui Li[2], Barbara M. Vertel[2] and Lisa Ebihara[1]

Departments of [1]Physiology & Biophysics and [2]Cell Biology & Anatomy, Rosalind Franklin University of Medicine and Science, North Chicago, IL 60064, USA

Previous studies have shown that gap junctional channels formed from the lens connexins Cx50 (or its chicken orthologue, Cx45.6) and Cx43 exhibit marked differences in transjunctional voltage gating and unitary conductance. In the present study, we used the negatively charged dye, Lucifer Yellow (LY), to examine and compare quantitative differences in dye transfer between pairs of HeLa cells stably transfected with Cx45.6 or Cx43. Our results show that Cx45.6 gap junctional channels are three times less permeable to LY than Cx43 channels. Replacement of the N-terminus of Cx45.6 with the corresponding domain of Cx43 increased LY permeability, reduced the transjunctional voltage (V_j) gating sensitivity, and reduced the unitary conductance of Cx45.6–43N gap junctional channels. Further experiments, using a series of Alexa probes that had similar net charge but varied in size showed that the Cx45.6–43N had a significantly higher permeability for the two largest Alexa dyes than Cx45.6. These data suggest that the N-terminus plays a critical role in determining many of biophysical properties of Cx45.6 gap junctional channels, including molecular permeability and voltage gating.

(Received 18 May 2006; accepted after revision 23 August 2006; first published online 24 August 2006)
Corresponding author L. Ebihara, Department of Physiology and Biophysics, Rosalind Franklin University of Medicine and Science, 3333 Green Bay Road, North Chicago, IL 60064, USA. Email: lisa.ebihara@rosalindfranklin.edu

Gap junctions allow the exchange of ions and other small molecules between neighbouring cells and thus can coordinate electrical and metabolic processes within a syncytial tissue. Most vertebrate gap junctions are formed from a family of closely related membrane proteins called connexins. Three different connexins are found in the mammalian lens: Cx43, Cx50 and Cx46 (Beyer *et al.* 1987; Paul *et al.* 1991; White *et al.* 1992). These connexins show different but overlapping patterns of expression in the lens.

Gap junctional channels formed from different connexins have different biophysical properties, such as unitary conductance, voltage gating and molecular permeability. Previous studies have shown that gap junctions are permeable to a number of important biological signalling molecules such as cAMP, IP_3 and glutamate (Lawrence *et al.* 1978; Saez *et al.* 1989). Different connexin channels show significant differences in permeability to metabolites and second messengers (Goldberg *et al.* 1999, 2002; Niessen *et al.* 2000; Bevans *et al.* 1998; Bedner *et al.* 2006). For instance, by using cyclic nucleotide-gated channels to quantify gap junction-mediated diffusion of cyclic AMP, Bedner *et al.* (2006) showed that Cx43 gap junctional channels were about 5–6 times more permeable to cAMP than Cx32 or Cx45 channels, and more than 30 times more permeable than Cx36 channels.

To better understand the contribution of charge and steric hindrance to connexin selectivity, fluorescent tracers of different charge and size have been used (Elfgang *et al.* 1995; Veenstra *et al.* 1995; Cao *et al.* 1998; Trexler *et al.* 2000; Weber *et al.* 2004). These studies show that certain connexins such as Cx45 and Cx46 form gap junctional channels that are more permeable to the cationic dyes than to the anionic dyes, while other connexins such as Cx43 show little charge preference. Recently, Weber *et al.* (2004) quantitatively examined the size selectivity of homotypic and heterotypic gap junctional channels expressed in *Xenopus* oocyte pairs by using a series of Alexa probes that have a similar structure and charge, but differ in size. The results of this study suggest that the size cut-off limits of the connexin channels could be ranked as: Cx32 $\geq$ Cx43 $\gg$ Cx26 $\geq$ Cx40 $\approx$ Cx45 $\geq$ Cx37 (Weber *et al.* 2004).

Each connexin has four hydrophobic, transmembrane regions (M1–M4). The N- and C-termini as well as the central loop that connects M2 and M3 are located on the cytoplasmic side of the membrane (Zimmer *et al.* 1987; Goodenough *et al.* 1988; Hertzberg *et al.* 1988; Milks *et al.* 1988; Yancey *et al.* 1989). Mutagenesis studies suggest that

 DOI: 10.1113/jphysiol.2006.113837

the N-terminus plays a critical role in determining the biophysical properties of gap junctional channels. The amino terminus has been shown to act as the voltage sensor and determine the polarity of transjunctional voltage (V_j)-dependent gating of Cx32 and Cx26 (Verselis *et al.* 1994; Oh *et al.* 1999, 2000; Purnick *et al.* 2000*a*, 2000*b*). It also is an important determinant of unitary conductance and rectification (Oh *et al.* 1999). The first 10 amino acid residues of the N-terminus of Cx32 have been proposed to lie within the channel pore and form the channel vestibule (Purnick *et al.* 2000*a*,*b*). Several recent studies suggest that the N-terminus may play a similar role for the α-group connexins (Musa *et al.* 2004; Tong *et al.* 2004; Srinivas *et al.* 2005).

In the present study, we examine the structural basis for the biophysical properties of two lens gap junctional proteins, chicken Cx45.6 (which is the chicken orthologue of Cx50) and rat Cx43, by constructing a chimera in which the N-terminus of Cx45.6 was exchanged with the corresponding domain of Cx43. Our results suggest that the N-terminus plays a critical role in determining many of biophysical properties of Cx45.6 gap junctional channels, including molecular selectivity for larger permeants.

Methods

Construction of Cx45.6–43N chimera

We constructed a Cx45.6–43NT chimera in which the N-terminus of chicken Cx45.6, delimited as Met1–Arg23 (Bennett *et al.* 1991), was replaced by the corresponding domain of rat Cx43. Two steps were used to generate the Cx45.6–Cx43NT chimera. (1) The region (Met1–Thr39) corresponding to the N-terminus and a portion of M1 of Cx45.6 was replaced with the corresponding region of Cx43. This exchange was facilitated by the presence of a naturally occurring *Pvu*II restriction site at the same position in the M1 domain of both Cx45.6 and Cx43 and a second naturally occurring *Pvu*II restriction site in the transcription vector, SP64T. (2) There are two amino acid differences in the M1 domain between the chimera constructed in the first step and Cx45.6. These two amino acids (Ser, Leu) of the chimera were replaced with the corresponding amino acids (Thr, Ile) of Cx45.6 by PCR mutagenesis using the QuikChange Site-Directed Mutagenesis Kit (Stratagene) and the primers: sense 5′-GGGAAGGTGTGGCTGACAGTGCTCTTCATATTC-AGAATCCTGATCCTGGGGACAGCTG-3′; and antisense 5′-CAGCTGTCCCCAGGATCAGGATTCTGAATATGAA-GAGCACTGTCAGCCACACCTTCCC-3′. The construct was fully sequenced (DNA Sequencing and Synthesis Facility, Iowa State University, Ames, IA, USA) to ensure that PCR amplification did not introduce random mutations.

Transient transfection of connexins in N2A cells

N2A mouse neuroblastoma cells were grown in Dulbecco's modified Eagle medium containing high glucose with 2 mM L-glutamine and no sodium pyruvate (Invitrogen, Carlsbad, CA, USA), supplemented with 10% fetal bovine serum, 100 u ml^{-1} penicllin G, and 100 μg ml^{-1} streptomycin sulphate, in a humidified atmosphere of 5% CO_2 at 37°C. For transient transfection, 1 μg of chicken Cx45.6, rat Cx43 or Cx45.6–Cx43N was cotransfected with 1 μg of enhanced green fluorescence protein (EGFP) cDNA into N2A mouse neuroblastoma cells using Superfect Transfection Reagent (Qiagen, Valencia, CA, USA) according to the manufacturer's protocol. Patch-clamp experiments were conducted 18 h later on EGFP-positive cell pairs.

Stable transfection of connexins in HeLa cells

A clone of HeLa cells essentially devoid of connexins was provided by V.K. Verselis (Albert Einstein College of Medicine, Bronx, NY, USA). Stable HeLa cell lines expressing chicken Cx45.6, rat Cx43 or Cx45.6–43N were generated using the Flp-In System (Invitrogen, Carlsbad, CA, USA) following the manufacturer's protocol. The stably transfected cells were selected and maintained in cell culture medium containing 300 μg ml^{-1} hygromycin.

Immunofluorescence localization

HeLa cells stably expressing Cx45.6, Cx43 and Cx45.6–Cx43N were seeded on glass coverslips (gelatinized, carbon-coated) at 20% confluence. At 2 days post-plating, cells were washed with phosphate-buffered saline (PBS), fixed in methanol at −20°C for 10 min, and stored in methanol at −4°C prior to immunofluorescent staining.

The polyclonal rabbit primary antibodies include anti-Cx45.6 antibody (provided by Dr Jean X. Jiang (University of Texas Health Science Center, San Antonio, TX, USA) against the C-terminus of Cx45.6, and anti-Cx43 antibody (Zymed Laboratories South San Francisco CA, USA) against the C-terminus of Cx43. Coverslips with fixed cells were washed three times with PBS for 5 min, followed by incubation with primary antibodies (1 : 200 diluted) at 37°C for 2 h. Then the cells were washed with PBS for at least 30 min and incubated in secondary antibody (Texas red-conjugated goat antirabbit IgG, Jackson ImmunoResearch Laboratories; 1 : 50 diluted) at 37°C for 1 h. After extensive PBS washes over 30 min, coverslips were mounted onto glass slides. The specimens were examined, and images were recorded through a Leica DMRB microscope equipped with a Hamamatsu CCD camera driven by the Openlab imaging program (Improvision).

Electrophysiological recording and analysis of gap junctional channels expressed in N2A cells

Junctional currents were obtained using the dual whole-cell patch-clamp technique as previously described (Xu *et al.* 2002). Computer-controlled patch-clamp amplifiers (MultiClamp 700 A, Molecular Devices, Sunnyvale, CA, USA) were used to control membrane potential and measure gap junctional currents. The resistance of patch pipettes was 4–6 MΩ when filled with standard internal solution. The standard internal solution contained (mM): 130 CsCl, 10 EGTA, 0.5 $CaCl_2$, 3 MgATP, 2 Na_2ATP, 10 Hepes, pH 7.4. The extracellular solution contained (mM) 140 NaCl, 2 CsCl, 1 $MgCl_2$, 5 Hepes, 4 KCl, 5 dextrose, 2 pyruvate, 1 $BaCl_2$, PH 7.4. Both cells of a EGFP-positive pair were initially held at 0 mV. A series of 8 s voltage-clamp pulses ranging between 100 mV and −100 mV in 10 mV decrements were applied to one cell, while the other cell was held constant at 0 mV and the junctional current was recorded from the non-pulsed cell. The normalized steady state conductance ($G_{j,ss}$) was calculated by dividing steady state junctional current ($I_{j,ss}$) by initial junctional current ($I_{j,Institute}$). The relationship between $G_{j,ss}$ and V_j was described and fitted by two-state Boltzmann equation:

$$G_{j,ss} = \{(G_{max} - G_{min})/(1 + \exp(A(V_j - V_0)))\} + G_{min} \quad (1)$$

where G_{max} is the maximum normalized conductance; G_{min} is the minimum normalized conductance; A is a parameter which represents the steepness of G–V curve and V_0 is the voltage when the $G_{j,ss}$ is half of its maximum value.

Single junctional channel currents were recorded from cell pairs having only one or two active gap junctional channels. The amplitude of single channel current was measured from all-amplitude histogram after fitting the patch clamp records by the sum of Gaussians. Data were obtained and analysed using PCLAMP 9.2 (Molecular Devices) and Sigma Plot 8.0 (SPSS, Chicago, IL, USA) software. All the experiments were conducted at room temperature (20–22°C). Results were presented as mean ± S.E.M.

Dye permeability measurements

Dye permeability through gap junctional channels was studied in stably transfected HeLa cell pairs. The concentration of LY (MW 457, 2 negative charges) dissolved in standard internal solution was 2 mmol l^{-1}. The Alexa dyes (Molecular Probes, Eugene, OR, USA) including Alexa 350 (MW 350, 1 negative charge), Alexa488 (MW 570, 1 negative charge) and Alexa 594 (MW 760, 1 negative charge) were also dissolved in pipette solution to reach a concentration of 1 mmol l^{-1}. The pH of all the dye containing solutions was 7.4. The resistance of patch pipettes ranged between 1 and 1.5 MΩ. Fluorescence was visualized using a Nikon Eclipse TE2000 inverted microscope equipped with an epi-fluorescence attachment (Nikon, Melville, NY, USA). Cells were excited with light from a mercury lamp after passing through appropriate bandpath filters. Image acquisition and analysis were performed using a Spot RT CCD camera (Diagnostic Instruments, Sterling Heights, MI, USA) and v3.5 Spot (Diagnostic Instruments) and Image J software (National Institutes of Health, Bethesda, DC, USA). To determine the relationship between the concentration of fluorescent dye and fluorescence intensity, a calibration curve for the camera was constructed by placing a 10 μl drop of a known concentration of LY on a coverslip and placing a second coverslip over it. Images were taken near the centre of the drop using a fixed exposure time for various concentrations of LY. The images were corrected for background intensity. The resultant calibration curve was linear for LY concentrations less than 2 mM (Fig. 7*B*).

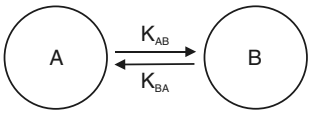

Figure 1. Two-compartment model

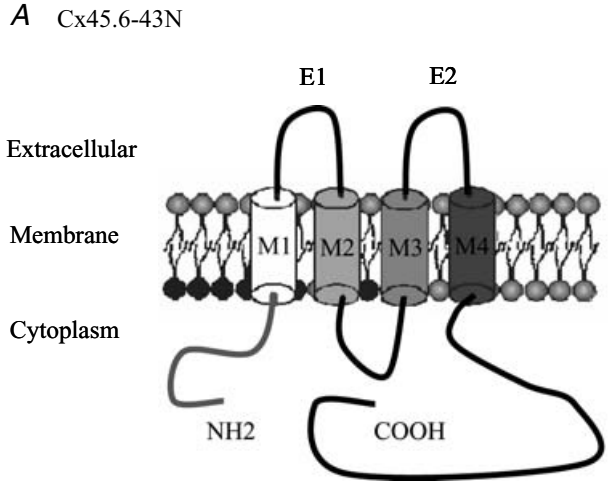

B

ChCx45.6 : MGDWSF LGNI LEQVN EQSTVI GR
RCx43 : MGDWS ALGKLLDK VQAY STAGGK

Figure 2. Membrane topology of Cx45.6–43 N
A, schematic representation and membrane topology of the chimeric gap junctional protein, Cx45.6–43 N, made by swapping the N-terminus between Cx45.6 (black) and Cx43 (red). *B*, alignment of Cx45.6 and Cx43 amino acid sequences of the N-terminus.

Table 1. Boltzmann parameters of connexins expressed in transiently transfected N2A cells

Cx	A (mV^{-1})	V_0 (mV)	G_{min}	G_j (nS)*	Number of cell pairs
Cx45.6	0.231	39.4	0.28	3.14 ± 0.37	4
Cx43	0.141	44.13	0.34	3.35 ± 0.24	4
Cx45.6–43N	0.115	52.68	0.40	2.00 ± 0.28	6

*Values are means ± S.E.M.

To quantitatively measure dye transfer, dye was loaded into one cell of the cell pair via the patch pipette in the whole-cell configuration. A series of negative current pulses were applied to the donor cell immediately after rupturing the membrane to increase the rate of dye loading into the donor cell. Images were collected at 1 min intervals for 6 min. The relative concentration of dye in the donor and recipient cells was determined at different time intervals by measuring the fluorescence intensity in a representative region of each cell and dividing it by the fluorescent intensity of the donor cell measured 6 min after patch rupture. At the end of the experiment, a second pipette was patched on the dye recipient cell in whole-cell mode and G_j was determined.

To estimate the fluorescent dye permeability through gap junction channels, the dye transfer data were fitted to the two-compartment kinetic model shown in Fig. 1 using Micro Math Scientist 3.0 software (Micromath Research, St Louis, MI, USA).

In this model, the concentration of dye in the recipient cell as a function of time is described by the differential equation:

$$Y'_B = K_{AB}(Y_A - Y_B) \quad (2)$$

where K_{AB} is the rate constant for dye passage through the gap junction (in units of min^{-1}), Y_A is the concentration of dye in the dye donor cell, and Y_B is the concentration of dye in the dye recipient cell. For the purpose of determining K_{AB}, the time course of Y_A could be reasonably well approximated by a monoexponential or sigmoidal function.

K_{AB} is related to the permeability coefficient, P, by

$$P = (V/A) \times K_{AB} \quad (3)$$

where A is the area of the gap junction and V is the cell volume. In our calculations, we assumed that all of the HeLa cells had the same cell volume ($V = 0.75$ pl). All the

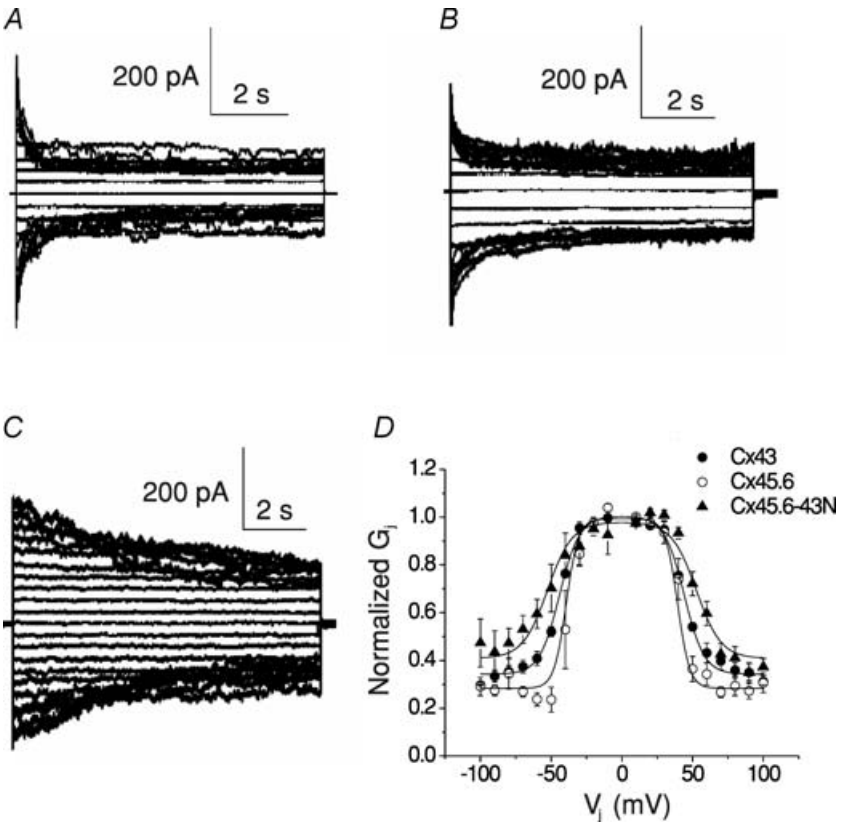

Figure 3. Voltage-dependent gating properties of homotypic gap junctional channels formed from Cx45.6, Cx43 or Cx45.6–43N
A–C, junctional current traces recorded from cell pairs expressing Cx45.6 (*A*), Cx43 (*B*) or Cx45.6–43N (*C*) in response to 8 s transjunctional voltage-clamp steps between +100 and −100 mV in 10 mV decrements. Holding potential = 0 mV. *D*, normalized steady-state gap junctional conductance (G_{jss}) as a function of transjunctional voltage (V_j) for Cx45.6 (○), Cx43 (●) and Cx45.6-Cx43N (▲). Points represent the mean ± S.E.M. The continuous lines represent the best fit of the data to a Boltzmann equation.

dye studies were performed at $V_j \approx 0$ mV. At this potential, there was no substate occupancy and the open probability of the gap junctional channels was close to 1.0 (see supplementary Fig. S1, which is published as supporting information on the J Physiol website). Similar results have been previously reported for hCx50 (Xu *et al.* 2002), mouse Cx50 (Srinivas *et al.* 1999) and rat Cx43 (Valiunas *et al.* 2002). Under these conditions, the number of functional gap junctional channels, $N = G_j/\gamma_j$. Therefore the single channel permeability

$$(\mathrm{AP})_{\mathrm{pore}} = V K_{\mathrm{AB}}/N \quad (4)$$

One complication in the analysis was that the measured value of junctional conductance ($G_{j,m}$) was smaller than the true value of junctional conductance ($G_{j,t}$) due to the presence of a resistance ($R_{s)}$ in series with the junctional resistance (R_j), which could account for a significant fraction of the voltage drop across the clamping electrodes. Assuming the membrane resistance (R_m) to be infinite, the relationship between $G_{j,t}$ and $G_{j,m}$ could be described by:

$$G_{j,t} = G_{j,m}(R_s + R_j)/R_j \quad (5)$$

To correct for this problem, the true value of G_j was estimated from the measured value by fitting the K_{AB}–$G_{j,m}$ curves to the following equations:

$$G_{j,m} = R_j/(R_j + R_s) \times G_{j,t} \quad (6)$$

$$K_{AB} = AG_{j,t} \quad (7)$$

where A is the slope factor, R_j is the true value of junctional resistance, R_s is the effective series resistance, and $G_{j,t}$ is the true value of G_j after correction for series resistance. The corrected value of junctional conductance ($G_{j,t}$) was then used to calculate the number of channels in a gap junction (N).

Results

Exchanging the N-terminus alters voltage gating

To examine the role of the N-terminus in determining the biophysical properties of Cx45.6 and Cx43 gap junctional channels, we constructed a chimeric gap junctional protein (Cx45.6–Cx43N) in which the N-terminus of Cx45.6 was replaced with the corresponding domain of Cx43. The membrane topology of Cx45.6–Cx43N is shown in Fig. 2*A*. Figure 2*B* shows a sequence alignment of the N-terminal domain of Cx45.6 and Cx43.

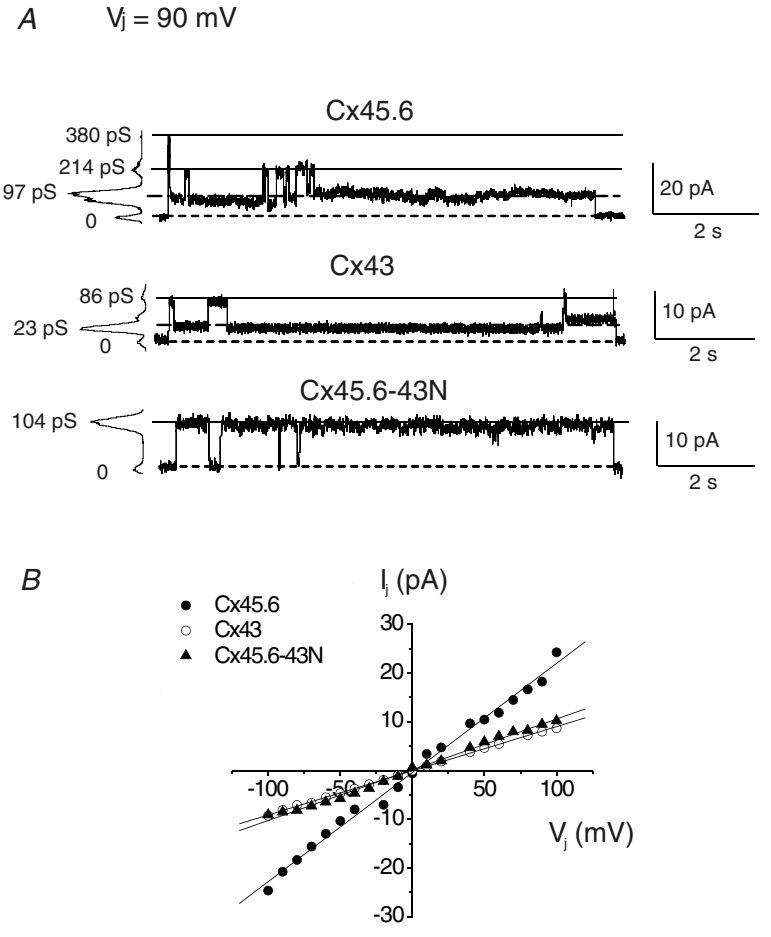

Figure 4. Single channel properties of Cx45.6, Cx43 and Cx45.6–43N gap junctional channels
A, records of single channel currents observed in pairs of N2A cells transfected with Cx45.6, Cx43 or Cx45.6–43N at $V_j = 90$ mV. Cx45.6–43N channels exhibit prolonged open times compared to Cx43 or Cx45.6. *B*, unitary *I–V* relationships of the Cx45.6, Cx43 and Cx45.6–43N gap junctional channels recorded in *A*. The slope conductance of Cx45.6–43N resembles that of Cx43.

Figure 3 shows families of macroscopic junctional current traces and corresponding isochronal G_j–V_j curves recorded from N2A cell pairs transiently transfected with Cx45.6, Cx43 or Cx45.6–43N. For all three connexins, the quasi-steady-state G_j was maximal at 0 mV and decreased at large transjunctional voltages (V_j) of either polarity. However, Cx45.6 and Cx43 gap junctional channels were more sensitive to V_j than channels composed of Cx45.6–43N. To quantify these differences in V_j sensitivity, the G_j–V_j curves were fitted to a two-state Boltzmann equation (Table 1). The voltage sensitivity of the connexin channels could be ranked in decreasing order as: Cx45.6 ($V_0 = 39.4$ mV, $A = 0.231$) > Cx43 ($V_0 = 44.13$ mV, $A = 0.141$) > Cx45.6–Cx43N ($V_0 = 52.68$ mV, $A = 0.115$). The three connexins also exhibited differences in kinetic properties. Cx45.6–43N channels inactivated more slowly at larger V_j values, compared to Cx45.6 or Cx43. These results suggest that the N-terminus plays an important role in determining the voltage-gating properties of Cx45.6 gap junctional channels.

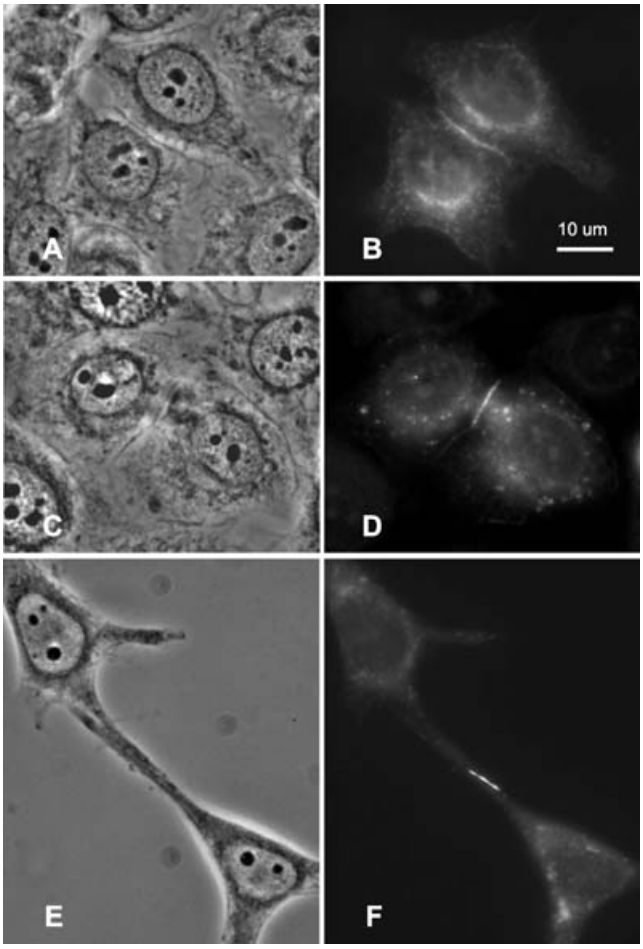

Figure 5. Immunolocalization of connexins in HeLa cells
Representative HeLa cells stably transfected with Cx45.6 (*A* and *B*), Cx43 (*C* and *D*) and Cx45.6–43N (*E* and *F*) are shown. Immunolocalized connexin is substantial at apposing cell membranes in regions of long gap junctions formed between the two adjacent cells of each cell pair. The connexin proteins were observed in the cytoplasm as well (*B*, *D* and *F*). Corresponding phase contrast images are shown (*A*, *C* and *E*).

Exchanging the N-terminus alters single channel conductance

Figure 4 shows single gap junctional currents recorded at $V_j = 90$ mV and corresponding unitary *I–V* curves for Cx45.6, Cx43 and Cx45.6–43 N. Cx45.6–43N channels exhibited prolonged open times compared to Cx43 or Cx45.6. Nearly all of the Cx45.6–43N gating transitions occurred between the main open state and the fully closed state. The unitary I_j–V_j relationship for Cx45.6–43N was linear over the voltage range between −100 mV and +100 mV, and had a slope conductance ($\gamma_{j,main}$) of 101 ± 3.1 pS ($n = 6$), which was very similar to the value of γ_j for Cx43 (90 ± 0.44 pS, $N = 3$) but half as large as that for Cx45.6 ($\gamma_j = 202 \pm 9.7$ pS, $N = 4$). These data indicate that the N-terminus is also an important determinant of single channel conductance.

Exchanging the N-terminus alters molecular permeability

To evaluate whether exchanging the N-terminus of Cx45.6 alters the molecular permeability properties of Cx45.6 gap junctional channels, we initially used the negatively charged dye, Lucifer Yellow (LY). The dye permeability experiments were performed on stably transfected HeLa cell pairs. Expression of the connexins was verified by immunofluorescence analyses with specific antibodies to the corresponding connexins. HeLa cell clones transfected with Cx45.6, Cx43 or Cx45.6–43N displayed immunoreactivity at the appositional plasma membranes as well as intracellularly, confirming that the expressed connexins reached the cell surface and formed gap junctional plaques, as illustrated in Fig. 5.

To measure dye transfer, LY was loaded into one cell of the cell pair via the patch pipette in the whole-cell configuration. Figure 6 shows fluorescent images of the time course of LY transfer recorded from three cell pairs transfected with Cx45.6, Cx43 or Cx45.6–Cx43N. To facilitate comparison of the relative rates of dye transfer, all of the images were taken from cell pairs that had similar values of G_j (∼40 nS). After 6 min of LY loading, the dye intensity in the recipient cell of both the Cx43 and Cx45.6–43N cell pairs was much stronger than that in the Cx45.6 cell pair. These data suggest that movement of LY through Cx43 and Cx45.6–43N gap junctional channels is faster than that through Cx45.6 channels.

Figure 7*A* shows plots of relative dye intensity as a function of time in the donor (open symbols) and recipient (filled symbols) cells for the three cell pairs shown in Fig. 6. The continuous lines were the best

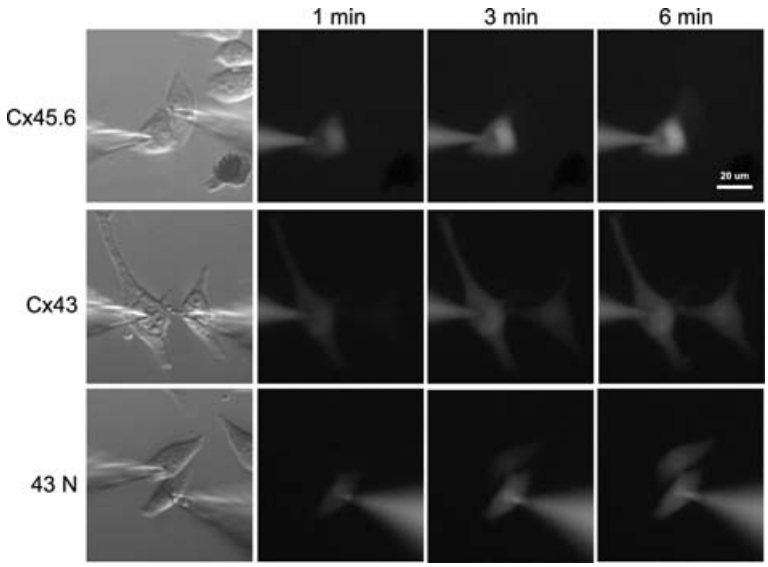

Figure 6. LY flux between pairs of Cx45.6, Cx43 or Cx45.6–43N HeLa cells
Epifluorescence micrographs are shown at 1, 3 and 6 min following patch rupture from cells pairs with similar values of $G_{j,m}$ (Cx45.6 40 nS; Cx43 40 nS; Cx45.6–43N 43 nS).

fit of the relative fluorescent intensity in the recipient cell to a two-compartment model. The rate constants for transfer of LY were: $K_{AB} = 0.03\ min^{-1}$ for Cx45.6, $K_{AB} = 0.21\ min^{-1}$ for Cx43, and $K_{AB} = 0.233\ min^{-1}$ for Cx45.6–43 N. The LY transfer data are summarized in Fig. 8*A*, which shows plots of K_{AB} *versus* $G_{j,m}$ for each connexin. Note that the relationship between K_{AB} and the measured value of G_j ($G_{j,m}$) deviated from linearity at larger values of $G_{j,m}$. We fitted each of these curves using a simple voltage divider model in which it was assumed that K_{AB} was directly proportional to the true value of junctional conductance ($G_{j,t}$), and thus any deviation from linearity was due to the presence of a resistance (R_s) in series with R_j. Using this model, which had only one free parameter, R_s, we could obtain very good fits of the data and reasonable estimates for R_s suggesting that this model could account for the behaviour of our data. In Fig. 8*B*, K_{AB} was replotted as a function of the corrected value of G_j ($G_{j,t}$) estimated using this model. The data for Cx43, Cx45.6 and Cx45.6–43N cell pairs were well described by a first-order regression with $r^2 = 0.99$, 0.86, and 0.99, respectively. The slopes of the curves for Cx45.6–43N and Cx43 were much steeper than that for Cx45.6, suggesting that LY could move through Cx43 and Cx45.6–43N channels faster than through Cx45.6 channels. From these data, the mean single channel permeability $(AP)_{pore}$ for each connexin was determined (Table 2). The mean value of $(AP)_{pore}$ for Cx45.6 was significantly less than the value of $(AP)_{pore}$ for Cx43 or Cx45.6–43 N.

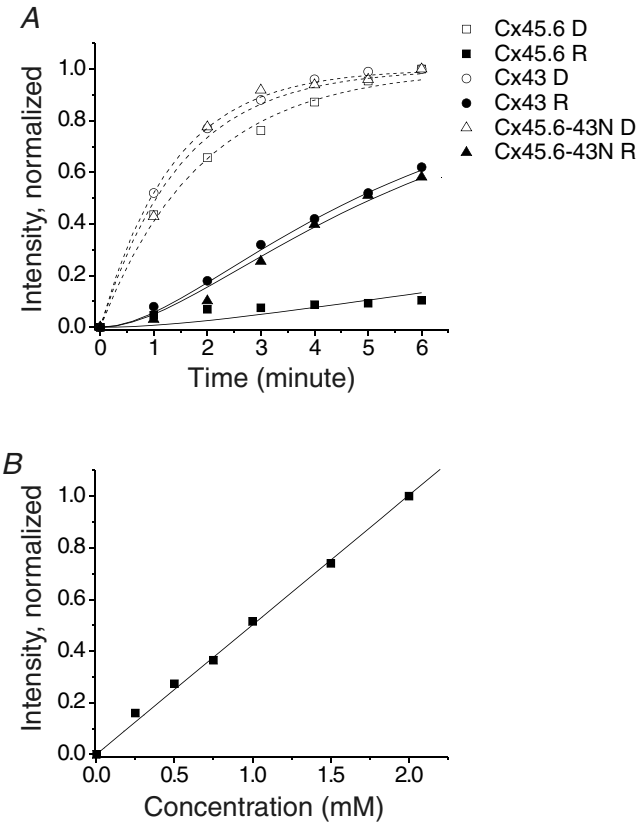

Figure 7. Time course of LY transfer through Cx45.6, Cx43 and Cx45.6–43N gap junctions
A, plots of relative fluorescence intensity *versus* time for dye donor cells (open symbols) and dye recipient cells (filled symbols) for the three cell pairs shown in Fig. 5. The continuous lines represent the best fit of the data to a two-compartment model with $r^2 = 0.99$ for Cx45.6, $r^2 = 0.97$ for Cx43 and $r^2 = 0.96$ for Cx45.6–43N.
B, calibration curve for the CCD camera. The continuous line is a first-order regression, with $r^2 = 0.99$.

Exchanging the N-terminus alters the size exclusion limit of Cx45.6 gap junctional channels

To examine if swapping the N-terminus altered LY permeability by increasing the size exclusion limit of

the Cx45.6–43N channels, we tested the ability of the wild-type and chimeric gap junctional channels to transfer three Alexa dyes (Alexa 350, MW 350; Alexa 488, MW 570; Alexa 594, MW 760) that had similar charge and molecular structure, but ranged in size from MW 350–760. Figure 9*A*–*C* shows representative fluorescent images for the time courses of dye transfer for each Alexa dye in cell pairs expressing Cx45.6, Cx43 or Cx45.6–43N. To facilitate comparison of the relative rates of dye transfer, all the images were taken from cell pairs that had similar values of G_j.

Figure 10 shows plots of relative dye intensity as a function of time in the donor and recipient cells for the cell pairs shown in Fig. 9. The continuous lines were the best fit of the fluorescent intensity data to a two-compartment model. The rate constants for dye transfer through Cx45.6 gap junctions decreased as the size of the dye increased, with values of $K_{AB} = 0.3247$ min^{-1} for Alexa 350, $K_{AB} = 0.044$ min^{-1} for Alexa 488 and $K_{AB} = 0$ for Alexa 594. In contrast, all three Alexa dyes transferred through Cx43 and Cx45.6–43N gap junctions at significant rates.

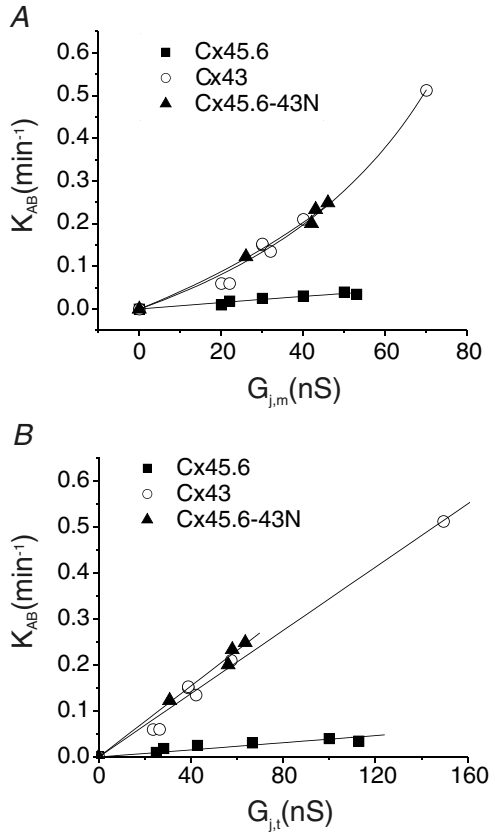

Figure 8. Relationship between rate constants of LY transfer and G_j

A, plots of K_{AB} *versus* the measured value of G_j ($G_{j,m}$) for Cx45.6 (■), Cx43 (○) and Cx45.6–43N (▲). The continuous lines represent the best fit of the data to eqns (6) and (7). The best fit values for series resistance (R_s) were 7.4 MΩ for Cx43 and 5.87 MΩ for Cx45.6–43 N, respectively. These values were very similar to the sum of the access resistances of the two patch electrodes measured experimentally ($R_s = 8.16 \pm 0.84$ MΩ). The value of R_s for Cx45.6 could not be accurately determined due to increased scatter in the data as a consequence of the low intensity of the signal. *B*, plots of K_{AB} *versus* the value of G_j corrected for series resistance ($G_{j,t}$). For the Cx45.6 data, R_s was assumed to be 8 MΩ. The continuous lines correspond to a first-order regression, with r^2 values of 0.86 for Cx45.6, 0.99 for Cx43 and 0.99 for Cx45.6–43 N.

Table 2. Single channel permeabilities ($\times 10^{-10}$ mm^3 min^{-1}) for LY through connexin channels

Cx	Cx45.6	Cx43	Cx45.6–43N
LY	0.79 ± 0.08 (6)	2.2 ± 0.16 (7)*	2.93 ± 0.08 (4)*

Values are mean ± S.E.M. of $(AP)_{pore}$ (units of 10^{-10} mm^3 min^{-1}). Number of cell pairs used in calculating permeability are shown in parentheses. The $(AP)_{pore}$ of Cx43 and Cx45.6–43N were significantly different from Cx45.6 when evaluated with a student's *t* test: $^*P < 0.001$.

Figure 11 shows plots of K_{AB} *versus* the corrected value of gap junctional conductance ($G_{j,t}$) for each of the Alexa dyes. The data for Cx45.6, Cx43 and Cx45.6–43N cell pairs were well described by a first-order regression. To compare quantitatively the permeability of the three Alexa dyes through different connexin channels, the single-channel permeability $(AP)_{pore}$ was determined. The results of these calculations are summarized in Table 3. The single-channel permeability of Cx45.6 for Alexa 350 was about three times higher than that for Alexa 488. Cx45.6 channels were impermeable to Alexa 594. In contrast, Cx43 channels showed similar single-channel permeabilities for both Alexa 350 and Alexa 594. The single-channel permeability of Cx43 for Alexa 488 was about two times higher than that for Alexa 350. The single-channel permeabilities of Cx45.6–43N for the Alexa dyes more closely resemble those of Cx43. One difference between Cx43 and Cx45.6–43N channels was that the single-channel permeability of Cx43 channels for Alexa 488 was significantly higher than that of Cx45.6–43N ($P < 0.01$).

Discussion

Several recent studies have shown that the N-terminus plays an important role in determining the voltage-gating properties and unitary conductance of different connexin channels. Our results suggest that the N-terminus also plays an important role in determining the molecular permeability and size exclusion limits of Cx45.6 gap junctional channels. Replacement of the N-terminus of Cx45.6 by the corresponding domain of Cx43 (Cx45.6–43N) decreased the unitary gap junctional conductance by twofold, and increased the permeability of the channel to LY. Further experiments, using a series

of Alexa probes that had similar net charge but varied in size showed that the Cx45.6–43N had a significantly higher permeability for the two largest Alexa dyes than Cx45.6.

The mechanisms underlying the differences in molecular permeability properties could involve steric factors. These factors include the length and average diameter of the pore, as well as more localized constrictions. In the present study, we find an inverse relationship between molecular size exclusion limits and the single channel conductance of Cx45.6 and Cx45.6–43N channels, suggesting that the differences in single channel conductance and permeability cannot be accounted for by a change in the average diameter of the pore. Rather, the presence of the N-terminus within the cytoplasmic vestibule of the pore might cause a more localized constriction that could restrict the passage of larger molecules such as Alexa 488 or Alexa 594 but have little effect on conductance. A similar inverse relationship has been seen for other connexin channels, such as Cx26 and Cx32, where Cx26, which has the smaller pore, has the greater unitary conductance (Bevan *et al.* 1998; Weber *et al.* 2004).

Electrostatic factors could also cause alterations in single channel conductance and molecular permeability. These factors include interaction of the charged permeant with the wall of the pore, and concentration of cations within the channel vestibule. Comparison of the amino acid sequence of the N-terminus of Cx45.6 with the homologous amino acid sequence of Cx43 reveals 11 amino acid substitutions, with three involving (acidic–basic) charge differences. Exchanging the N-terminus of Cx45.6 for the corresponding domain of Cx43 would make the N-terminus less negative, and thus might reduce accumulation of cations near the cytoplasmic mouth of the channel and result in a decrease in single channel conductance as observed experimentally, provided that the channel exhibits substantial selectivity for cations over anions elsewhere in the permeation pathway. The ionic selectivity of Cx45.6 gap junctional channels has not been investigated. However, gap junctional channels composed of a closely related connexin (Cx46) have been reported to select for K^+ over Cl^- at a 7 : 1 ratio (Trexler *et al.* 2000). An analogous mechanism has been proposed to account for the large conductance of BK channels (Brelidze *et al.* 2003).

Previous studies suggest there are other domains of the connexin in addition to the N-terminus that can influence the unitary conductance and molecular selectivity of large molecules. These domains include the carboxyterminal half of the first transmembrane-spanning domain (M1) (Hu & Dahl, 1999; Hu *et al.* 2006; Ma & Dahl, 2006; Kronengold *et al.* 2003; Oh *et al.* 1997), the aminoterminal half of the first extracellular domain (E1) (Kronengold *et al.* 2003), the carboxyl terminus (CT) (Fishman *et al.* 1991; Lampe *et al.* 2000) and possibly the third transmembrane-spanning domain (M3) (Skerrett

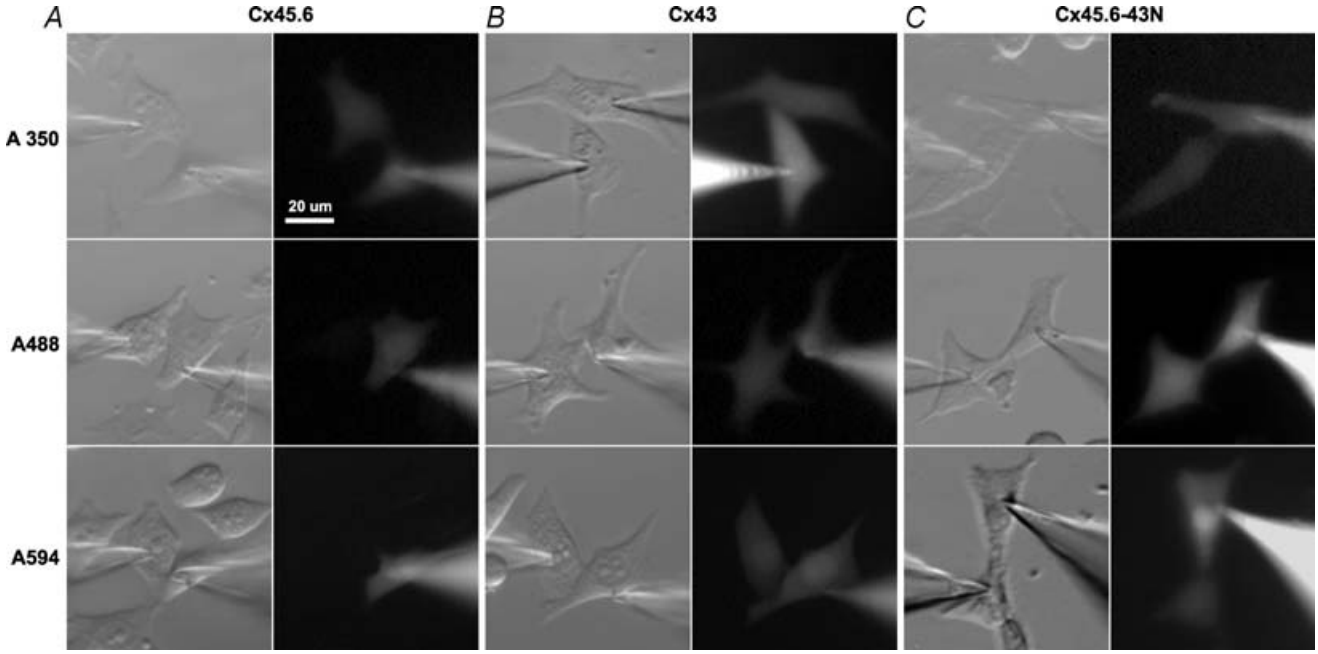

Figure 9. Alexa dye flux between pairs of Cx45.6 (*A*), Cx43 (*B*) and Cx45.6–43N (*C*) HeLa cells
Representative images of the intercellular diffusion of the three Alexa dyes are shown for homotypic Cx45.6, Cx43 and Cx45.6–43N gap junctions. The epifluorescence images were collected 6 min after patch rupture. All of the cell pairs have similar values of G_j (Cx45.6–50 nS; Cx43–45 nS; Cx45.6–43N ~40 nS).

et al. 2002). The carboxyterminal half of M1 has been recently shown to be a critical determinant of both size exclusion limits and the unitary conductance of connexin channels. Interestingly, chimeras in which the M1 domain of Cx46 was replaced with the corresponding domain of Cx32, or vice versa, showed a correlation between unitary conductance and size exclusion limits as would be predicted to occur in a cylindrical channel with exclusively steric constraints (Ma & Dahl, 2006). Another important domain is the aminoterminal half of E1. Kronengold *et al.* (2003) showed that fixed charges within E1 influence the single channel conductance, rectification and selectivity of Cx46 hemichannels. This behaviour may be hemichannel specific since these charged residues would be located near the centre of the pore of a gap junctional channel, and therefore could no longer concentrate ions as they do at the extracellular mouth of a hemichannel.

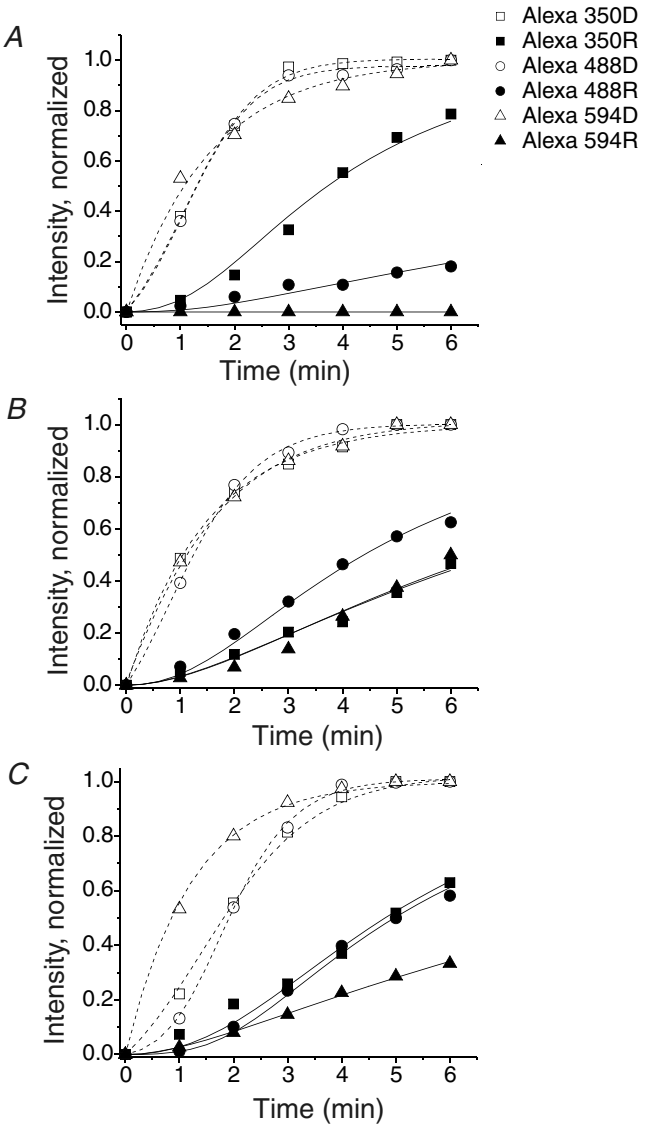

Figure 10. Time course of dye transfer for the three Alexa dyes through Cx45.6 (*A*), Cx43 (*B*) and Cx45.6–43N (*C*) gap junctions
Plots of relative fluorescence intensity *versus* time for dye donor cells (open symbols) and dye recipient cells (filled symbols) for the cell pairs shown in Fig. 8. The continuous lines represent the best fit of the data to a two-compartment model.

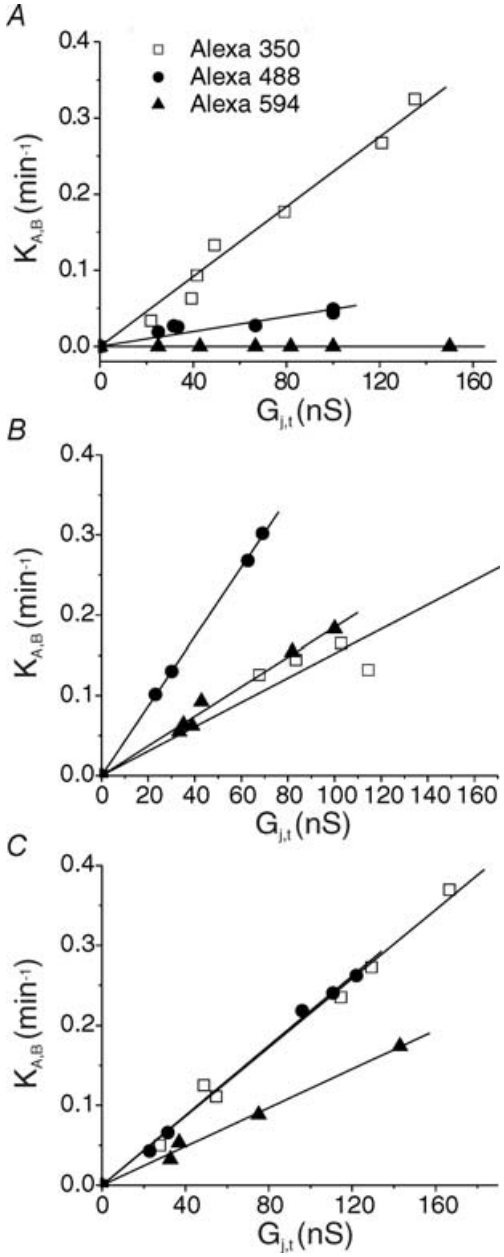

Figure 11. Relationship between rate constants of intercellular transfer of the three Alexa dyes and G_j
A, plots of K_{AB} *versus* the corrected value of G_j ($G_{j,t}$) through Cx45.6 gap junctions: Alexa 350 (□), Alexa 488 (●), Alexa 594 (▲). The continuous lines correspond to a first-order regression with r^2 values of 0.98 for Alexa 350, 0.88 for Alexa 488. *B*, plots of K_{AB} *versus* the corrected value of G_j ($G_{j,t}$) through Cx43 gap junctions: Alexa 350 (□), Alexa 488 (●), Alexa 594 (▲). The continuous lines correspond to a first-order regression, with r^2 values of 0.97 for Alexa 350, 0.98 for Alexa 488 and 0.99 for Alexa 594. *C*, plots of K_{AB} *versus* corrected value of G_j ($G_{j,t}$) through Cx45.6–43N gap junctions: Alexa 350 (□), Alexa 488 (●), Alexa 594 (▲). The continuous lines correspond to the first-order regression, with r^2 values of 0.99 for all three Alexa dyes.

Table 3. Single channel permeabilities ($\times 10^{-10}$ mm^3 min^{-1}) for Alexa dyes through connexin channels

Cx	Alexa 350	Alexa 488	Alexa 594
45.6	3.24 ± 0.24 (7)	0.94 ± 0.12 (6)	0 (6)
43	1.14 ± 0.08 (5)*	2.93 ± 0.02 (4)*†	1.23 ± 0.06 (6)*
45.6–43 N	1.6 ± 0.08 (6)*	1. 6 ± 0.05 (5)*	0.91 ± 0.07 (4)*

Values are mean ± S.E.M. of $(AP)_{pore}$ (units of 10^{-10} mm^3 min^{-1}). Number of data sets used in calculating permeability shown in parentheses. The $(AP)_{pore}$ of Cx43 and Cx45.6–43N were significantly different from Cx45.6 when evaluated with a student's *t* test: $^*P < 0.001$. The $(AP)_{pore}$ of Cx43 was significantly different from Cx45.643N when evaluated with a student's *t* test: $\dagger P < 0.001$.

In addition to altering the single channel conductance and molecular permeability, exchanging the N-terminus slowed the inactivation kinetics and reduced the steady-state V_j of the Cx45.6–43N gap junctional channels. It has been proposed that the N-terminus may lie within the pore where it can sense the membrane field and act as a voltage sensor for V_j gating of gap junctional channels (Verselis *et al.* 1994). The movement of the N-terminus toward the cytoplasm in response to a transjunctional voltage difference is thought to close the channel. In our case, the reduction in transjunctional voltage sensitivity of Cx45.6–43N gap junctional channels could be due to the fact that the N-terminus of Cx43 is more positively charged than that of Cx45.6.

Despite the importance of the N-terminus, it cannot account for all of the differences in voltage-gating properties between Cx45.6 and Cx43, suggesting that there are other critical determinants in Cx43 that influence voltage gating. Comparison of the voltage-gating properties of wild-type Cx43 and Cx45.6–43N gap junctional channels showed several interesting differences: (1) Cx45.6–43N gap junctional channels were less sensitive to junctional voltage, and inactivated more slowly than Cx43 when V_j was high; (2) the open time of single channel current of Cx45.6–43N was longer than Cx43 at high V_j; (3) nearly all of the Cx45.6–43N gating transitions occurred between the main open state and the fully closed state, whereas for Cx43 channels, transitions between the main open state and the residual state predominated. Interestingly, the voltage-gating properties of Cx45.6–43N junctional channels show a strong resemblance to those of the 'tailless' mutant rat Cx43 (Revilla *et al.* 1999; Moreno *et al.* 2001). The carboxyl terminus of Cx43 has been proposed to be the effector of fast V_j-dependent gating of Cx43 channels. Although it is thought to interact with the pore-affiliated regions to open or close the pore, it is neither a determinant for slow V_j-dependent gating of Cx43 nor a component of the ion-conducting pathway. Unlike Cx43, the voltage-gating properties of Cx45.6 channels do not appear to involve interactions of the carboxyl terminus with the mouth of the pore. Truncation of the carboxyl tail of the human orthologue of Cx45.6, human Cx50, had no effect on its voltage-gating properties or single channel conductance (Xu *et al.* 2002). In contrast, replacing the N-terminus of Cx45.6 with the N-terminus of Cx43 completely transformed the voltage-gating properties and single channel conductance of Cx45.6 into those of the 'tailless' mutant of Cx43. These results suggest that the N-terminus is a major determinant of the unitary conductance and V_j-gating properties of Cx45.6 channels and may be also involved in determining the slow V_j-gating properties of Cx43 channels.

References

Bedner P, Niessen H, Odermatt B, Kretz M, Willecke K & Harz H (2006). Selective permeability of different connexin channels to the second messenger cyclic AMP. *J Biol Chem* **281**, 6673–6681.

Bennett MV, Barrio LC, Bargiello TA, Spray DC, Hertzberg E & Saez JC (1991). Gap junctions: new tools, new answers, new questions. *Neuron* **6**, 305–320.

Bevans CG, Kordel M, Rhee SK & Harris AL (1998). Isoform composition of connexin channels determines selectivity among second messengers and uncharged molecules. *J Biol Chem* **273**, 2808–2816.

Beyer EC, Paul DL & Goodenough DA (1987). Connexin43: a protein from rat heart homologous to a gap junction protein from liver. *J Cell Biol* **105**, 2621–2629.

Brelidze TI, Niu X & Magleby KL (2003). A ring of eight conserved negatively charged amino acids doubles the conductance of BK channels and prevents inward rectification. *Proc Natl Acad Sci U S A* **100**, 9017–9022.

Cao F, Eckert R, Elfgang C, Nitsche JM, Snyder SA, Hulser DF, Willecke K & Nicholson BJ (1998). A quantitative analysis of connexin-specific permeability differences of gap junctions expressed in HeLa transfectants and *Xenopus* oocytes. *J Cell Sci* **111**, 31–43.

Elfgang C, Eckert R, Lichtenberg-Frate H, Butterweck A, Traub O, Klein RA, Hulser DF & Willecke K (1995). Specific permeability and selective formation of gap junction channels in connexin-transfected HeLa cells. *J Cell Biol* **129**, 805–817.

Fishman GI, Moreno AP, Spray DC & Leinwand LA (1991). Functional analysis of human cardiac gap junction channel mutants. *Proc Natl Acad Sci U S A* **88**, 3525–3529.

Goldberg GS, Lampe PD & Nicholson BJ (1999). Selective transfer of endogenous metabolites through gap junctions composed of different connexins. *Nat Cell Biol* **1**, 457–459.

Goldberg GS, Moreno AP & Lampe PD (2002). Gap junctions between cells expressing connexin 43 or 32 show inverse permselectivity to adenosine and ATP. *J Biol Chem* **277**, 36725–36730.

Goodenough DA, Paul DL & Jesaitis L (1988). Topological distribution of two connexin32 antigenic sites in intact and split rodent hepatocyte gap junctions. *J Cell Biol* **107**, 1817–1824.

Hertzberg EL, Disher RM, Tiller AA, Zhou Y & Cook RG (1988). Topology of the Mr 27 000 liver gap junction protein. Cytoplasmic localization of amino- and carboxyl termini and a hydrophilic domain which is protease-hypersensitive. *J Biol Chem* **263**, 19105–19111.

Hu X & Dahl G (1999). Exchange of conductance and gating properties between gap junction hemichannels. *FEBS Lett* **451**, 113–117.

Hu X, Ma M & Dahl G (2006). Conductance of connexin hemichannels segregates with the first transmembrane segment. *Biophys J* **90**, 140–150.

Kronengold J, Trexler EB, Bukauskas FF, Bargiello TA & Verselis VK (2003). Single-channel SCAM identifies pore-lining residues in the first extracellular loop and first transmembrane domains of Cx46 hemichannels. *J Gen Physiol* **122**, 389–405.

Lampe PD, TenBroek EM, Burt JM, Kurata WE, Johnson RG & Lau AF (2000). Phosphorylation of connexin43 on serine368 by protein kinase C regulates gap junctional communication. *J Cell Biol* **149**, 1503–1512.

Lawrence TS, Beers WH & Gilula NB (1978). Transmission of hormonal stimulation by cell-to-cell communication. *Nature* **272**, 501–506.

Ma M & Dahl G (2006). Cosegregation of permeability and single-channel conductance in chimeric connexins. *Biophys J* **90**, 151–163.

Milks LC, Kumar NM, Houghten R, Unwin PNT & Gilula NB (1988). Topology of the 32-kD liver gap junction protein determined by site-directed antibody localizations. *EMBO J* **7**, 2967–2975.

Moreno AP, Chanson M, Elenes S, Anumonwo J, Scerri I, Gu H, Taffet SM & Delmar M (2001). Role of the carboxyl terminal of connexin43 in transjunctional fast voltage gating. *Circ Res* **90**, 450–457.

Musa H, Fenn E, Crye M, Gemel J, Beyer EC & Veenstra RD (2004). Amino terminal glutamate residues confer spermine sensitivity and affect voltage gating and channel conductance of rat connexin40 gap junctions. *J Physiol* **557**, 863–878.

Niessen H, Harz H, Bedner P, Kramer K & Willecke K (2000). Selective permeability of different connexin channels to the second messenger inositol 1,4,5-trisphosphate. *J Cell Sci* **113**, 1365–1372.

Oh S, Abrams CK, Verselis VK & Bargiello TA (2000). Stoichiometry of transjunctional voltage-gating polarity reversal by a negative charge substitution in the amino terminus of a connexin32 chimera. *J Gen Physiol* **116**, 13–31.

Oh S, Ri Y, Bennett MV, Trexler EB, Verselis VK & Bargiello TA (1997). Changes in permeability caused by connexin 32 mutations underlie X-linked Charcot–Marie–Tooth disease. *Neuron* **19**, 927–938.

Oh S, Rubin JB, Bennett MV, Verselis VK & Bargiello TA (1999). Molecular determinants of electrical rectification of single channel conductance in gap junctions formed by connexins 26 and 32. *J Gen Physiol* **114**, 339–364.

Paul DL, Ebihara L, Takemoto LJ, Swenson KI & Goodenough DA (1991). Connexin46, a novel lens gap junction protein, induces voltage-gated currents in nonjunctional plasma membrane of *Xenopus* oocytes. *J Cell Biol* **115**, 1077–1089.

Purnick PE, Benjamin DC, Verselis VK, Bargiello TA & Dowd TL (2000b). Structure of the amino terminus of a gap junction protein. *Arch Biochem Biophys* **381**, 181–190.

Purnick PE, Oh S, Abrams CK, Verselis VK & Bargiello TA (2000a). Reversal of the gating polarity of gap junctions by negative charge substitutions in the N-terminus of connexin 32. *Biophys J* **79**, 2403–2415.

Revilla A, Castro C & Barrio LC (1999). Molecular dissection of transjunctional voltage dependence in the connexion-32 and connexion-43 junctions. *Biophys J* **77**, 1374–1383.

Saez JC, Connor JA, Spray DC & Bennett MV (1989). Hepatocyte gap junctions are permeable to the second messenger, inositol 1,4,5-trisphosphate, and to calcium ions. *Proc Natl Acad Sci U S A* **86**, 2708–2712.

Skerrett IM, Aronowitz J, Shin JH, Cymes G, Kasperek E, Cao FL & Nicholson BJ (2002). Identification of amino acid residues lining the pore of a gap junction channel. *J Cell Biol* **159**, 349–360.

Srinivas M, Costa M, Gao Y, Fort A, Fishman GI & Spray DC (1999). Voltage dependence of macroscopic and unitary currents of gap junction channels formed by mouse connexin50 expressed in rat neuroblastoma cells. *J Physiol* **517**, 673–689.

Srinivas M, Kronengold J, Bukauskas FF, Bargiello TA & Verselis VK (2005). Correlative studies of gating in Cx46 and Cx50 hemichannels and gap junction channels. *Biophys J* **88**, 1725–1739.

Tong JJ, Liu X, Dong L & Ebihara L (2004). Exchange of gating properties between rat cx46 and chicken cx45.6. *Biophys J* **87**, 2397–2406.

Trexler EB, Bukauskas FF, Kronengold J, Bargiello TA & Verselis VK (2000). The first extracellular loop domain is a major determinant of charge selectivity in connexin46 channels. *Biophys J* **79**, 3036–3051.

Valiunas V, Beyer EC & Brink PR (2002). Cardiac gap junction channels show quantitative differences in selectivity. *Circ Res* **91**, 104–111.

Veenstra RD, Wang HZ, Beblo DA, Chilton MG, Harris AL, Beyer EC & Brink PR (1995). Selectivity of connexin-specific gap junctions does not correlate with channel conductance. *Circ Res* **77**, 1156–1165.

Verselis VK, Ginter CS & Bargiello TA (1994). Opposite voltage gating polarities of two closely related connexins. *Nature* **368**, 348–351.

Weber PA, Chang HC, Spaeth KE, Nitsche JM & Nicholson BJ (2004). The permeability of gap junction channels to probes of different size is dependent on connexin composition and permeant-pore affinities. *Biophys J* **87**, 958–973.

White TW, Bruzzone R, Goodenough DA & Paul DL (1992). Mouse Cx50, a functional member of the connexin family of gap junction proteins, is the lens fiber protein MP70. *Mol Biol Cell* **3**, 711–720.

Xu X, Berthoud VM, Beyer EC & Ebihara L (2002). Functional role of the carboxyl terminal domain of human connexin 50 in gap junctional channels. *J Membr Biol* **186**, 101–112.

Yancey SB, John SA, Lal R, Austin BJ & Revel JP (1989). The 43-kD polypeptide of heart gap junctions: immunolocalization, topology and functional domains. *J Cell Biol* **108**, 2241–2254.

Zimmer DB, Green CR, Evans WH & Gilula NB (1987). Topological analysis of the major protein in isolated intact rat liver gap junctions and gap junction-derived single membrane structure. *J Biol Chem* **262**, 7751–7763.

Acknowledgements

We thank Dr V. K. Verselis (Albert Einstein College of Medicine, Bronx, NY, USA) for providing the parental HeLa cells, and Dr J. X. Jiang (University of Texas Health Science Center, San Antonio, TX, USA) for providing antibodies for Cx45.6. This work was supported by NIH grant EY10589 (to L. Ebihara).

Supplemental material

The online version of this paper can be accessed at:
DOI: 10.1113/jphysiol.2006.113837
http://jp.physoc.org/cgi/content/full/jphysiol.2006.113837/DC1
and contains supplemental material consisting of a figure.
This material can also be found as part of the full-text HTML version available from http://www.blackwell-synergy.com